



PAPER • OPEN ACCESS

Irradiation-induced enhancement of Fe and Al magnetic polarizations in Fe₆₀Al₄₀ films

To cite this article: A Smekhova *et al* 2024 *New J. Phys.* **26** 023036

View the [article online](#) for updates and enhancements.

You may also like

- [Spin-textured Volkov–Pankratov states and their tunnel magnetoresistance response](#)
Vivekananda Adak, Subhadeep Chakraborty, Krishanu Roychowdhury *et al.*
- [Spin–orbit interaction enabled high-fidelity two-qubit gates](#)
Jiaan Qi, Zhi-Hai Liu and Hongqi Xu
- [Phonon and maxon instability in Bose–Einstein condensates with parity-time symmetric spin–orbit coupling](#)
Jieli Qin, Lu Zhou and Guangjiong Dong



PAPER

Irradiation-induced enhancement of Fe and Al magnetic polarizations in Fe₆₀Al₄₀ films

OPEN ACCESS

RECEIVED
3 May 2019ACCEPTED FOR PUBLICATION
12 December 2023PUBLISHED
20 February 2024Original Content from
this work may be used
under the terms of the
[Creative Commons
Attribution 4.0 licence](#).Any further distribution
of this work must
maintain attribution to
the author(s) and the title
of the work, journal
citation and DOI.A Smekhova^{1,2,*}, Th Szyjka³, E La Torre³, K Ollefs³, B Eggert³ , B Cöster³, F Wilhelm⁴ , R Bali⁵, J Lindner⁵,
A Rogalev⁴, D Töbrens², E Weschke², C Luo^{2,6}, K Chen², F Radu², C Schmitz-Antoniak^{1,7} and H Wende³¹ Peter Grünberg Institut (PGI-6), Forschungszentrum Jülich, D-52425 Jülich, Germany² Helmholtz-Zentrum Berlin für Materialien und Energie (HZB), D-12489 Berlin, Germany³ Faculty of Physics and Center for Nanointegration Duisburg-Essen (CENIDE), University of Duisburg-Essen, D-47048 Duisburg, Germany⁴ European Synchrotron Radiation Facility (ESRF), BP 220, 38043 Grenoble Cedex 9, France⁵ Institut für Ionenstrahlphysik und Materialforschung, Helmholtz-Zentrum Dresden-Rossendorf, D-01328 Dresden, Germany⁶ Institute of Experimental Physics of Functional Spin Systems, Technical University Munich, 85748 Garching b. München, Germany⁷ Present address: TH Wildau—University of Applied Sciences, Hochschulring 1, 15745 Wildau, Germany.

* Author to whom any correspondence should be addressed.

E-mail: alevtina.smekhova@helmholtz-berlin.de**Keywords:** chemical disorder, ion-irradiation, XANES, XMCD, plasma treatmentSupplementary material for this article is available [online](#)**Abstract**

The rise of Fe magnetic moment, changes in Al electronic structure and a variation of Al magnetic polarization in thin films of transition metal aluminide Fe₆₀Al₄₀ have been probed through the order-disorder phase transition by soft x-ray absorption spectroscopy and x-ray resonant magnetic reflectivity in the extreme ultraviolet regime. In a course of the transition induced by 20 keV Ne⁺ irradiation with low fluences ($\sim 10^{14}$ ions cm⁻²), x-ray magnetic circular dichroism spectra taken at the Fe L_{2,3} absorption edges at room and low temperatures revealed a pronounced increase of Fe 3d states spin-polarization. X-ray resonant magnetic reflectivity applied to the Al L_{2,3} and Fe M_{2,3} edges allowed to detect the magnetic polarization of Al atoms in the films. The changes in Al electronic structure have been seen by alteration of Al K edge x-ray absorption near edge structure. A difference in anisotropy fields for films before and after irradiation has been observed by element-specific hysteresis loops recorded at low temperatures in absorption and reflection geometries at the Fe L_{2,3} and M_{2,3} edges, respectively. An attempt to reduce the top oxide layer by an inductively coupled hydrogen plasma has shown a possibility to recover the chemically ordered phase.

1. Introduction

The phenomenon of disorder-induced ferromagnetism in a series of transition metal alloys and thin films represented by an acquiring of ferromagnetic properties via destroying the structure is very appealing for the technological applications. It is known for decades that in e.g. Fe_{1-x}M_x systems (alloys and thin films) with M = Al, V, Cr or Rh, local configurations of Fe and M atoms play an important role in formation of the macroscopic magnetization [1–4]. Later on, it was shown that slight changes of the local environment performed by light ions beam mixing revealed technologically relevant outcomes like patterning of low roughness areas with increased magnetization and different coercivities in FeAl films [5], decrease of saturation fields and increase of giant magnetoresistance in Fe/Cr multilayers [6], and a visible shift of antiferromagnetic-ferromagnetic phase-transition temperature in FeRh [7].

A number of theoretical and experimental works have demonstrated that particularly in FeAl alloys, the competition between ferromagnetic (Fe–Fe) and antiferromagnetic (Fe–Al) exchange interactions between neighboring atoms, the number of Fe-Fe nearest-neighbors, unit cell changes, and the influence of further coordination shells result in a very complex formation mechanism of Fe magnetic moments [8–12] (and

references therein). Recent achievements in magnetic patterning of $\text{Fe}_{60}\text{Al}_{40}$ thin films by ion irradiation with low fluences [13], studies of magnetization reversal [14], a possibility to have tailored magnetic properties inside a chosen volume of the film [15], and a reversibility of the disordered states back to the initially ordered one by thermal annealing [16] provide a great perspective for constructing key blocks of prototyping complex magnetic devices. Besides, heating with laser pulses can modify significantly the magnetic properties at the surface of $\text{Fe}_{1-x}\text{Al}_x$ bulk alloy or thin film depending on number of pulses [17, 18], and allows to get back the ordered single domain state from the disordered one [18]. Although prior macroscopic, optical, photoelectron emission microscopy, Mössbauer spectroscopy [13, 15, 16], and recent hard x-ray absorption spectroscopy (XAS) [19] studies indicate important influence of created chemical disorder on static and dynamic magnetic properties, a better understanding of this phenomenon on atomistic scale is demanded. To this end, element-specific x-ray spectroscopy studies of electronic and magnetic properties associated with a particular local configuration created by ion irradiation with low fluences can be performed.

XAS is an effective tool to probe the environment of an absorbing atom as well as its electronic and magnetic properties on a local scale. The extended x-ray absorption fine structure (EXAFS) of K edges ($s \rightarrow p$ transitions) is a unique signature of the absorber embedded in a particular surrounding. Being very sensitive to the several first coordination shells of the chosen absorber, EXAFS oscillations provide information on the chemical nature of the nearest-neighbors, their coordination, distances from the absorbing atom and their thermal/static disorders. Main peculiarities of the electronic structure of absorbers can be taken from x-ray absorption near edge (XANES) region while the element-specific magnetic properties can be obtained by x-ray magnetic circular dichroism (XMCD) spectra e.g. at K, L and/or M edges.

A direct access to magnetism of d states which define magnetic properties of transition metals is provided by polarization-dependent XAS at $L_{2,3}$ absorption edges ($2p_{1/2,3/2} \rightarrow nd_{3/2,5/2}$ transitions). An opportunity to retrieve the magnetic moments in μ_{Bohr} units from experimental XMCD spectra separately for the spin and orbital contributions is given by the well established sum rules analysis [20, 21]. Thereby specific variations of Fe $3d$ spin polarization depending on irradiation fluence, and their changes with magnetic field and temperature can be probed.

Another element-specific technique—x-ray resonant magnetic reflectivity (XRMR) – is a well established tool to study buried layers and interfaces in the magnetic multilayer systems of nanometer sizes [22–25]. It is widely applied in the soft x-ray regime at the $L_{2,3}$ edges of transition metals or the $M_{4,5}$ edges of rare-earths, where the strong magneto-optical (MO) response exists. Employed in the extreme ultraviolet (XUV) energy range which covers $L_{2,3}$ edges of Al as well as $M_{2,3}$ edges of Fe, it could be used to disclose magnetic polarizations of Al atoms even through only a tiny Al signal is expected. An example of XRMR studies in XUV energy range with polarized x-rays from a synchrotron source can be found e.g. in [26, 27] and references therein.

In the present report, element-specific EXAFS, XANES and XMCD techniques at the Al K and Fe $L_{2,3}$ absorption edges have been applied to study consequential changes of local environment and related magnetic/electronic properties of Fe and Al atoms in bare $\text{Fe}_{60}\text{Al}_{40}$ thin films through the order-disorder phase transition induced by 20 keV Ne^+ ion irradiation. XRMR at the Al $L_{2,3}$ and Fe $M_{2,3}$ edges was used to probe the magnetic polarizations of Al atoms induced by Fe-Al hybridization and their antiferromagnetic coupling with iron moments. In addition, the possibility to recover the chemically ordered phase by a hydrogen plasma treatment has been explored.

2. Experimental details

2.1. Samples

As-deposited $\text{Fe}_{60}\text{Al}_{40}$ thin films of 40 nm thickness were prepared by magnetron sputtering at room temperature (RT) on $\text{SiO}_2/\text{Si}(001)$ substrates from a target of the same Fe-rich composition. The native oxide buffer layer was necessary to prevent an unfavorable silicide formation at the $\text{Fe}_{60}\text{Al}_{40}/\text{Si}$ interface during the annealing process in vacuum at 773 K (~ 1 h) to achieve the formation of the chemically ordered B2 phase. The chemically disordered A2 phases were created by further *ex situ* 20 keV Ne^+ irradiation with fluences of $(0.75 - 6) \times 10^{14}$ ions cm^{-2} . The film irradiated with the highest fluence of 6×10^{14} ions cm^{-2} is assigned to the fully disordered A2 state within the current manuscript. TEM images have shown that all samples have a top oxide layer of $\sim 3-4$ nm thickness [13]. More details about sample preparation and irradiation process could be found in [13, 16, 19].

2.2. X-ray measurements

Grazing incidence x-ray diffraction data (GIXRD) have been collected at the KMC-2 synchrotron beamline at Helmholtz-Zentrum Berlin (BESSY II, Berlin, Germany) [28]. The energy of the incoming x-rays was set to 8.048 keV, 1.5406 Å wavelength, corresponding to $\text{CuK}\alpha_1$ radiation. All data were collected by a Bruker

Vantec 2000 area detector at ambient conditions; the intensity of the primary beam was used for the normalization. Special care was taken of the vertical alignment of samples: for each individual film the sample position and the 0.5° incidence angle of the primary beam were adjusted with an accuracy of 0.01 mm and 0.01° , respectively, in order to avoid any deviations in sample tilting that would affect the results of measurements.

Soft x-ray absorption spectra have been recorded at the high-field end-station of UE46-PGM-1 beamline at Helmholtz-Zentrum Berlin (BESSY II, Berlin, Germany) [29, 30]. The geometry of the experiment was the same as in our previous studies [19] (45° of grazing incidence), but the signal was collected in the total electron yield (TEY) mode. XANES spectra at the Fe $L_{2,3}$ edges (~ 700 – 730 eV) have been measured with circularly polarized x-rays from the third harmonic of the elliptical undulator with 90% circular polarization either at room or low temperature of 5 K (LT). The XMCD spectra were taken by reversing the polarization of incoming x-rays while keeping the magnetic field fixed ($+1.8$ T) along the beam direction. TEY of the Pt coated Si mirror before the end-station was used for the normalization on the incoming photons intensity. EXAFS and XANES spectra at the Al K edge (~ 1550 – 1800 eV) were recorded at 5 K with horizontally polarized x-rays. To ensure a stable drain current of secondary electrons from the samples a small magnetic field of $+0.4$ T was applied.

The XRMF experiment at the Fe $M_{2,3}$ (~ 53 eV) and Al $L_{2,3}$ (~ 73 eV) absorption edges has been performed at VEK MAG end-station of PM2 beamline at Helmholtz-Zentrum Berlin (BESSY II, Berlin, Germany) [31]. The reflection spectra were recorded at 12.5 K for a 45° incidence geometry in magnetic fields of ± 1.8 T applied along the incident beam for two opposite circular polarizations of the incoming x-ray photons. The degree of circular polarization was set to 77%. The detected signal has been normalized on the incoming intensity measured by a Ta coated mesh upstream to the end-station in the diagnostic chamber. Element-specific MO hysteresis loops measured at several energies around the Fe $M_{2,3}$ and Al $L_{2,3}$ absorption edges have been used to prove the magnetic nature of the characteristic features in the asymmetry of the reflectivity spectra. The precisely confirmed position of the absorption edge of metallic Al has been checked by observing the absorption edge of the direct beam when passing through a $500 \mu\text{m}$ Al foil placed in front of a Si based detector.

3. Experimental results

3.1. GIXRD results

The *bcc* structure of all studied films and the presence of the structural $B2 \rightarrow A2$ phase transition is demonstrated by GIXRD data in figure 1. For the chemically ordered B2 phase the superlattice peak from (100) plane is clearly visible despite the Fe-rich stoichiometry forces 10% of Fe atoms to be on Al sublattice sites and the presence of slight tetragonal distortions. This peak is associated with the ordered fraction of the sample and could not be attributed to any Al- or Fe- oxides at the top of the films as well as SiO_2 buffer layer or Si substrate [13]. For A2 phases obtained by ion irradiation of $(0.75\text{--}6) \times 10^{14}$ ions cm^{-2} fluences this superlattice peak vanishes with fluence increasing and only the basic characteristic peaks related to diffraction from (110), (200) and (211) planes remain. The positions of these diffraction peaks show a well pronounced increase of the lattice parameter from $2.87(2)$ Å to $2.915(2)$ Å upon the irradiation.

3.2. EXAFS and XANES at K edges

Strong consequential changes of the local environment around Fe absorbers in $\text{Fe}_{60}\text{Al}_{40}$ films prepared by Ne^+ irradiation have been previously found by EXAFS at the Fe K edge at RT in [19]; the detailed study based on the EXAFS and wavelet analysis, first-principles density functional calculations as well as XMCD and magnetic multi-electronic excitations results at the Fe K edge can be found there. A short summary related to the structural EXAFS part can be also seen in Supplementary Material.

Complementary information about changes of the local environment through the phase transition could be retrieved from EXAFS spectra taken at the Al K edge; for this case the direct access to the neighborhood of Al absorbers is possible. The Al K edge EXAFS spectra recorded at low temperature for better visibility of expected difference between local environments in B2 and A2 states are shown in figure 2. Similarly to the Fe K edge the EXAFS oscillations are noticeably different for phases before and after the irradiation even through the Al atoms are much weaker backscatters. Moreover, at both edges EXAFS spectra show visibly dumped amplitudes for the fully disordered A2 phase.

Owing to the underlying SiO_2 buffer layer (150 nm) the EXAFS oscillations could be recorded only up to ~ 300 eV above the absorption edge due to the presence of intense Si K edge white line at ~ 1835 eV (see Supplementary Material). The EXAFS analysis performed for a so narrow energy range hardly provides a necessary precision in determination of the effective radial distances around Al absorbers and has been skipped. Nevertheless, a number of conclusions can be done by considering the Al K edge XANES region,

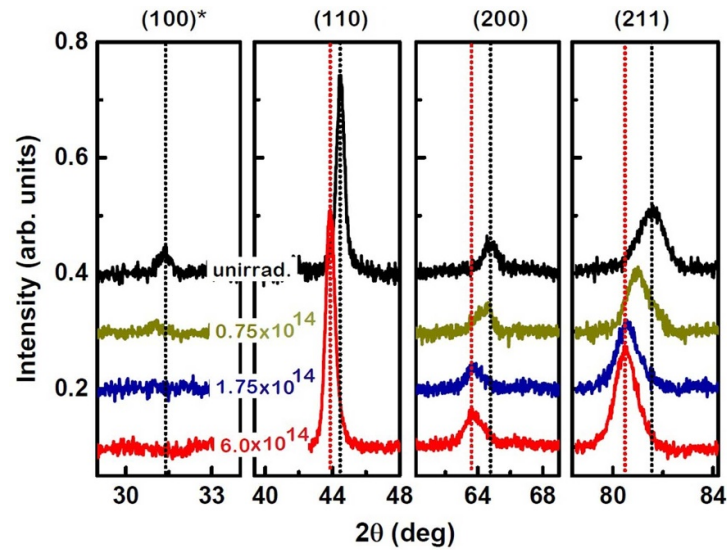


Figure 1. GIXRD data collected at room temperature for the ordered (B2) and the disordered (A2) states of $\text{Fe}_{60}\text{Al}_{40}$ thin films irradiated by 20 keV Ne^+ ions of indicated fluences in ions cm^{-2} units. The corresponding diffraction planes are indicated above the panels. The planes (100)* are associated with the ordered fraction of the sample. The experiment has been performed at the KMC-2 beamline of HZB.

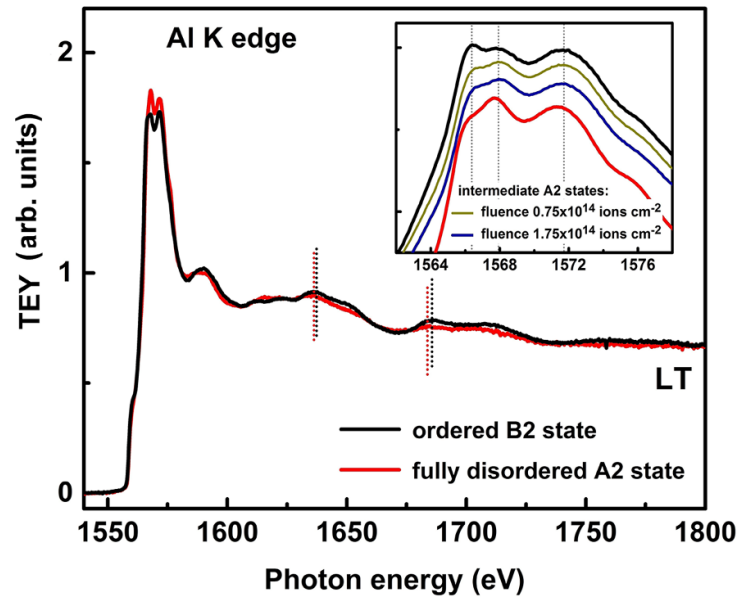


Figure 2. EXAFS spectra for the ordered (B2) and the fully disordered (A2) states of $\text{Fe}_{60}\text{Al}_{40}$ recorded at the Al K edge at 5 K. The fully disordered A2 state is represented by the sample irradiated with fluence of 6×10^{14} ions cm^{-2} . The inset shows the XANES spectra of two intermediate A2 states have been added, all spectra are shifted vertically for clarity. The experiment has been performed at the UE46-PGM-1 beamline of HZB.

where a prime distinction in absorption spectra exists (see inset in figure 2): for the ordered B2 phase a pronounced peak at ~ 1566 eV was found while for the studied A2 phases the intensity of the absorption spectrum at this particular energy is much smaller. It is clearly seen that the disordered A2 states created by Ne^+ irradiation with fluences of $(0.75 - 6) \times 10^{14}$ ions cm^{-2} reveal an essentially different electronic structure of Al as compared to the case of the chemically ordered B2 state. It also allows to assume that the main structural and electronic transformations related to $\text{B2} \rightarrow \text{A2}$ phase transition have been accomplished already at around 0.75×10^{14} ions cm^{-2} fluence, in agreement with GIXRD data.

XAS spectra of all considered states exhibit a clear shoulder at ~ 1559 eV. This energy is related to the absorption threshold of metallic Al in a pure metallic Al foil (*fcc* structure) [32, 33] showing the presence of non-oxidized Al in all studied samples. Nevertheless, Al in metallic foil exhibits a broad peak around 1565 eV while Al in the studied aluminide films shows a different near edge structure which overlaps with a strong

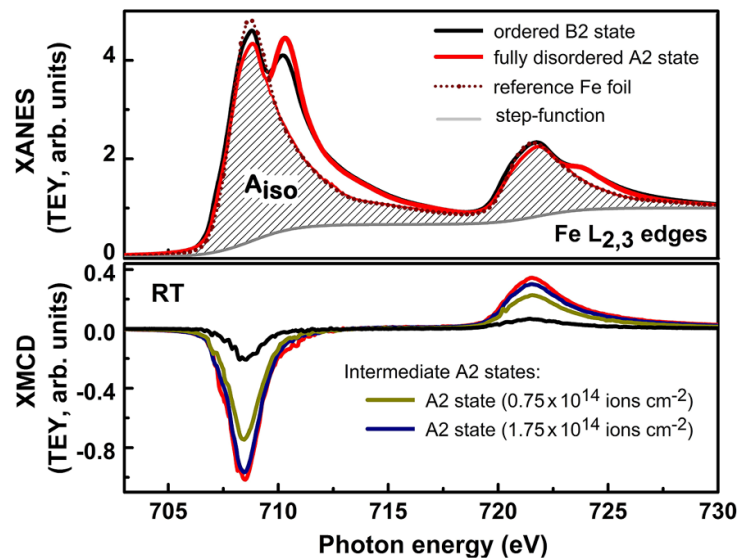


Figure 3. XANES (top) and XMCD (bottom) spectra for the ordered (B2) and the fully disordered (A2) states of $\text{Fe}_{60}\text{Al}_{40}$ films recorded at the $\text{Fe L}_{2,3}$ edges under +1.8 T magnetic field at RT together with XANES of a reference Fe foil spectra. The experiment has been performed at the UE46_PGM-1 beamline of HZB. The step function as $(2/3)/(1 + \exp(708.9 - E_{ph})) + (1/3)/(1 + \exp(721.9 - E_{ph}))$ estimates transitions into continuum (E_{ph} is the energy of incoming x-ray photons).

contribution from $\alpha\text{g} - \text{Al}_2\text{O}_3$ native oxide layer. Previously, the presence of a similar pronounced shoulder for the ordered B2 FeAl alloy and a distinctive feature between Al K edge near-edge structure for a pure Al and Al in Fe aluminide were demonstrated in [34] by electron energy-loss spectroscopy and *ab initio* local density approximation calculations.

According to studies of different Al oxides and minerals [32, 35–37], to the peak around 1566 eV a fraction of Al^{3+} ions in tetrahedral (T_d) coordination does contribute, whereas the two pronounced peaks at 1568 eV and 1572 eV with a possible bump around 1566 eV are associated with Al^{3+} ions in octahedral coordination (O_h). The relative intensities of these three peaks allow to assume that in our case the observed peak around 1566 eV is a superposition of contributions from metallic Al inside the films and from a small amount of Al^{3+} ions in tetrahedral (T_d) coordination in the top oxide layer.

The local surrounding of Al atoms in the studied $\text{Fe}_{60}\text{Al}_{40}$ films is significantly different as compared to the Al foil because they have different crystallographic structures (bcc contrary to fcc) and due to a predominant iron environment with a strong Al–Fe hybridization: for the ordered B2 phase (the ideal case) all Al absorbers are in the pure iron environment due to Fe-rich stoichiometry while for the disordered A2 phase the number of Al–Al next-neighbors are only 3.2 (according to the binomial distribution, see e.g. [19]). Thus, the near edge structure of Al absorption spectra is expected to be different from the spectra of Al foil and should vary significantly with changes in the chemical disorder under the irradiation. The reverse changes in the observed fine structure of Al K edge XANES region have been found for films after the hydrogen plasma treatment.

3.3. XANES and XMCD at the $\text{Fe L}_{2,3}$ edges

XANES spectra of the unirradiated and irradiated films recorded at the $\text{Fe L}_{2,3}$ absorption edges exhibit a clear oxidation peak as shown in figure 3(top) for the ordered B2 and the fully disordered A2 states while XMCD spectra for all studied films (see figure 3(bottom)) are represented by only a single contribution from the metallic iron sites. This is in agreement with the assumption that iron ions in the top oxide layer align antiferromagnetically and, thus, do not have a net magnetic moment. So, a rough separation between contributions from metallic iron and oxidized iron ions to XAS spectra might be possible. The amplitude of the XMCD signal associated with a metallic iron grows from its smallest value for the ordered B2 phase up to the largest value for the fully disordered one (A2) as expected [19].

The presence of the oxidation peak makes the determination of the magnetic moment absolute values via sum rules analysis rather problematic due to a not well defined isotropic absorption area (A_{iso}) associated with metallic iron sites. Nevertheless, even more complicated cases of iron/iron oxide core-shell nanoparticles and granular nanostructures (where besides oxidation peak in XANES the strong XMCD signal comes up from Fe^{2+} and Fe^{3+} ions in addition to metallic iron) could be treated due to a characteristic shape of the XMCD signal [38, 39]. The known ways for elimination of the native oxide layer like soft plasma

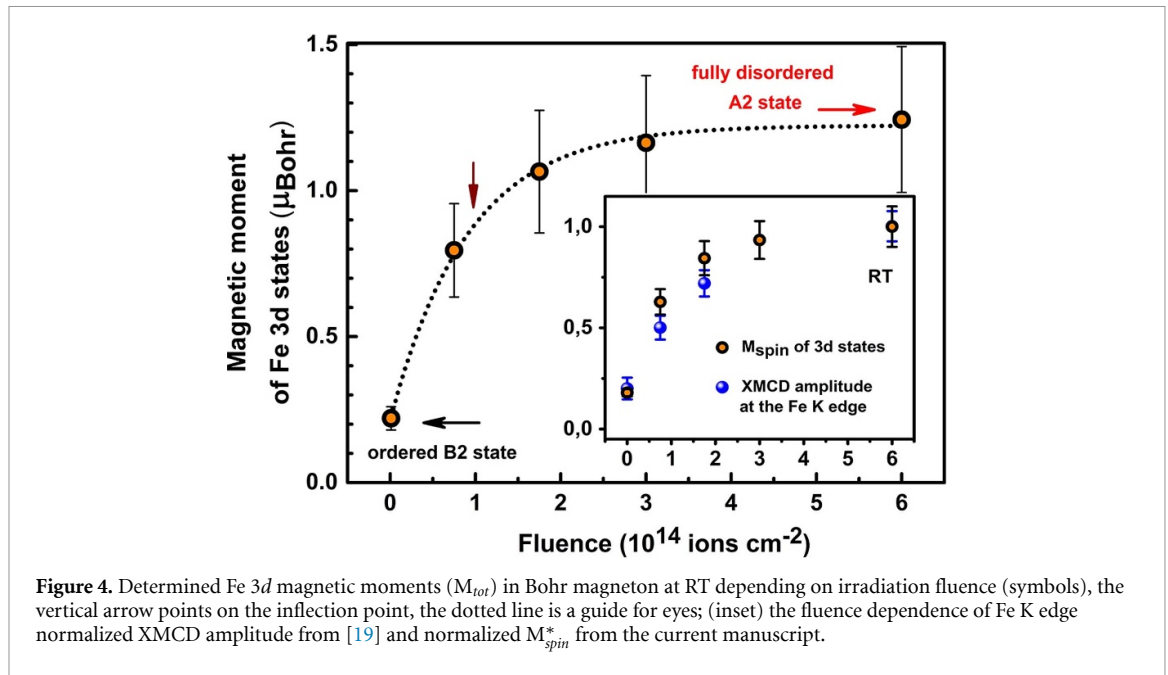


Figure 4. Determined Fe 3d magnetic moments (M_{tot}) in Bohr magneton at RT depending on irradiation fluence (symbols), the vertical arrow points on the inflection point, the dotted line is a guide for eyes; (inset) the fluence dependence of Fe K edge normalized XMCD amplitude from [19] and normalized M_{spin}^* from the current manuscript.

treatment [40, 41] and Ag^+ sputtering are not acceptable in our case since they affect the local coordination of atoms just below the oxide layer or need further annealing, respectively. That in turn alters significantly the magnetic properties of films prepared by ion-irradiation due to disruption of a characteristic depth-profile of the chemical disorder. Moreover, a reduction of Fe oxides from the top layer to metallic iron is followed by a small increase of the net magnetic moment due to spins that previously were coupled antiferromagnetically in the oxide. Two illustrative examples of the soft hydrogen plasma treatment influence on the resulting net magnetic moments are considered in the appendix. Meanwhile, using XAS spectra of the iron foil as a reference, an attempt to get the correct tendency of raising Fe magnetic moments depending on Ne^+ fluence could be done.

The isotropic absorption area A_{iso} necessary for further analysis was estimated as shown in figure 3(top) by a patterned area (for the A2 state). In such a way the contribution from the oxidized iron ions to the absorption spectra is strongly diminished while the main variations of the white line intensity related to the metallic iron in the film are preserved. Due to this procedure the obtained absolute values of magnetic moments are slightly reduced since the fraction of iron atoms that coupled antiferromagnetically within the top oxide layer still contributes to the rest of the absorption peak. Another variation in the isotropic absorption area that affects the estimation of magnetic moments relates to the hybridization effect between Fe 3d and Al p states and acts in the opposite direction by increasing the values of the magnetic moments. In the case of $Fe_{60}Al_{40}$ films this variation could be up to 10% according to our rough estimations. However, the resulting systematic error is of the same order for all studied films and is not crucial for the main conclusions.

The sum rules analysis with considering the isotropic absorption area as mentioned above has revealed the pronounced increase of Fe total magnetic moment (M_{tot}) within the chosen fluence range. The obtained M_{tot} in units of μ_{Bohr} are plotted in figure 4. An essential growth of the magnetic moment takes place already at small fluences and then tends to saturate. Qualitatively, the same fluence dependence was obtained by macroscopic measurements of MO Kerr effect (MOKE) [13]. The inflection point of the fluence dependence recorded by XMCD (approx. 1×10^{14} ions cm^{-2}) is shifted to higher fluences in comparison with one measured previously by MOKE (0.45×10^{14} ions cm^{-2}). We relate this shift to a characteristic depth-profile of disordering created by 20 keV Ne^+ ions and only a surface sensitivity of soft x-rays: the main contribution (63%) to the signal measured by secondary electrons (TEY) stems from ~ 2 nm depths due to a short electron mean free path [42–44], the rest of the signal comes from deeper depths up to ~ 7 nm [45]. According to simulations with the Transport of ions in matter program package (TRIM) [46], the degree of the disorder in $Fe_{60}Al_{40}$ films (in terms of displacements per atom, dpa) at the probing depth of MOKE (~ 15 nm) is larger than at the maximal probing depth of XMCD; thus, higher fluences are needed to induce the same degree of the chemical disorder and related magnetic moment closer to the surface. A direct comparison of fluence dependences obtained by XMCD technique and MOKE can be found in the Supplementary Material.

Taking into account the depth-profile of the disordering created by ion-irradiation is crucial for comparison of results obtained by methods with different probing depths. The strong deviation in results taken by SQUID magnetometry and soft x-rays XMCD technique at 20 K was previously found during the

Table 1. The values of Fe 3*d* total magnetic moment (M_{tot}) per 3*d* hole, the number of 3*d* holes, M_{tot} , the effective spin (M_{spin}^*) and orbital (M_{orb}) magnetic moments estimated by sum rules analyses applied to the XMCD spectra recorded at RT from unirradiated sample and samples irradiated by $(0.75 - 6) \times 10^{14}$ ions cm^{-2} fluences. The amplitudes of the XMCD signal at the Fe K edge (at 7117 eV) are from [19].

	Ordered B2 state	Intermediate A2 states			Fully disordered A2 state	Fe bulk <i>bcc</i>
Fluence [<i>ions cm</i> ⁻²]	–	0.75×10^{14}	1.75×10^{14}	3×10^{14}	6×10^{14}	–
RT						
M_{tot} [μ_{Bohr} / 3 <i>d</i> hole]	0.06(1)	0.23(5)	0.30(6)	0.32(6)	0.37(7)	0.65 ^a
Number of 3 <i>d</i> holes ^(*)	3.6(4)	3.5(4)	3.5(4)	3.6(4)	3.4(3)	3.4 ^a
M_{tot} [μ_{Bohr}]	0.22(4)	0.80(16)	1.07(21)	1.16(23)	1.24(25)	2.2 ^a
M_{spin}^* [μ_{Bohr}]	0.21(4)	0.74(15)	1.00(20)	1.10(22)	1.18(24)	2.02 ^a
M_{orb} [μ_{Bohr}]	< 0.01	0.05(1)	0.07(1)	0.06(1)	0.06(1)	0.18 ^a
XMCD at the Fe K edge	0.18(4)	0.48(10)	0.75(15)	–	1.00(20)	~1 ^b ; 1.5 ^c

^a Stöhr and Siegmann [44].

^b Pizzini et al [48].

^c Mathon et al [49].

*The number of 3*d* holes was estimated from the comparison of the isotropic absorption area for the film and the reference spectra of Fe foil, assuming the number of 3*d* holes for the reference spectra as 3.4.

attempt to measure the fluence dependence for Fe₄₇Rh₅₃ thin films about 80 nm thickness on MgO substrate, where the ferromagnetic order was created by 10 MeV I⁺ ions irradiation with fluences of $\sim 10^{13}$ ions cm^{-2} [47].

The inset in figure 4 shows the normalized amplitudes of the Fe K-edge XMCD signal (at 7117 eV) from [19] together with M_{spin}^* of Fe 3*d* states from the current report for different fluences. The similarity in the shapes of aforementioned dependences is in agreement with the common assumption that the orbital polarization of delocalized Fe 4*p* states reflected in XMCD signal at the Fe K edge is mainly determined by the spin polarization of Fe 3*d* states through the exchange interaction with Fe 4*p* spin moment and further through a slight spin-orbit coupling of 4*p* states. A variation in a curvature of these dependences could be a result of different strengths of 4*p* – 3*d* hybridization in states created by different fluences. Also, an influence of different probing depths for exploiting detection modes (i.e. TFY and TEY for hard- and soft x-rays, respectively) can not be excluded.

The values of M_{tot} per 3*d* hole, the number of 3*d* holes, M_{tot} , the effective spin (M_{spin}^*) and orbital (M_{orb}) magnetic moments together with amplitudes of the XMCD signal taken from the Fe K edge (at 7117 eV) from [19] are presented in table 1 for a better comparison. The 3*d* magnetic moment for the fully disordered A2 state is approx. 57% of the Fe bulk values. This result is fully consistent with Mössbauer spectroscopy data from [9]. The values for the ordered and the fully disordered states are in good agreement with theoretical results calculated for these particular films in [19]. The major contribution into M_{tot} is an effective spin moment M_{spin}^* that contains the $\langle T_z \rangle$ term [21]. Even though this term could not be well estimated quantitatively, we assume that in our current study it could be neglected due to the cubic symmetry and the rather small spin-orbit coupling in Fe, so that M_{spin}^* is a good measure of the spin contribution to the total magnetic moment. The orbital contribution M_{orb} into the total magnetic moment is very weak, yet, all irradiated films have shown a visibly increased M_{orb} with a similar fluence-dependence as the magnetic multi-excitations peak integrated intensity measured at the Fe K edge [19].

Element-specific hysteresis curves (ESHC) for the unirradiated and the fully irradiated films measured in the same experimental geometry at the maximum of the XMCD signal (around 708 eV) at RT are presented in figure 5(top) in XMCD asymmetry units. XMCD asymmetry was calculated as $(P - M)/(P + M)$, where P and M are TEY for two opposite polarizations of the incoming x-ray photons. As follows from the figure, both films exhibit an open hysteresis loop with comparable coercive fields (~ 4 mT), but only the unirradiated film (the ordered B2 state) has a pronounced slope in the field dependence of the XMCD asymmetry while the fully disordered one (A2 state) shows the squared hysteresis with a clear saturation.

Low temperature XMCD measurements revealed an increase of XMCD amplitudes as compared to RT values for all considered states and a drastic change in the shape of the ESHC for the unirradiated sample, where a significant increase in the coercive field (up to ~ 80 mT at 5 K) has been found, while the shape of the ESHC for the fully irradiated sample stays nearly the same (see figure 5(bottom)). Such an increase in the coercivity at LT can be related to the dominantly ordered state of the unirradiated sample, which has only a small fraction of Fe-rich regions. This ordered state is mainly isotropic and suggests a broad distribution of

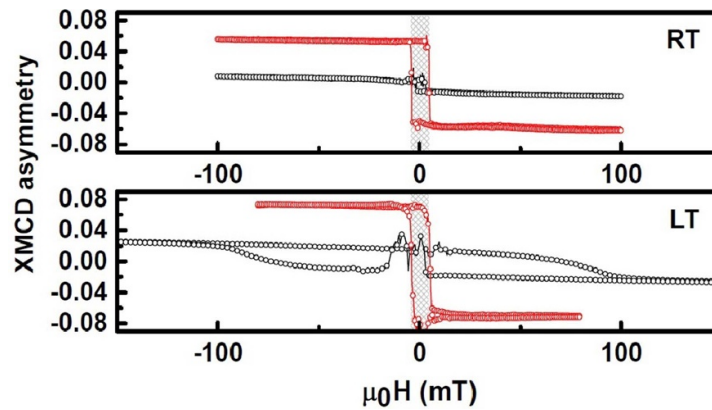


Figure 5. Element-specific hysteresis curves for the initially ordered and the fully disordered states (black curves for B2 and red curves for A2, respectively) of $\text{Fe}_{60}\text{Al}_{40}$ measured at the maximum of the XMCD signal around 708 eV at room (top) and low (bottom) temperatures. The region of the TEY instability is shown by patterned area. The experiment has been performed at the UE46_PGM-1 beamline of HZB.

the magnetic easy axes of film crystallites that are randomly oriented. This broad distribution is also responsible for the slope of the hysteresis at RT.

A possible influence of the film ageing due to a continuous air exposure on magnetic XMCD signal has been checked by recording XMCD spectra for the ordered and the fully disordered samples with a time delay of nine months after the prime studies. A magnetic signal variation within only 1% has been found. This variation could be attributed to the deviations in the detected secondary electrons yield due to an inhomogeneity of the top oxide layer and not to the magnetic ageing of films.

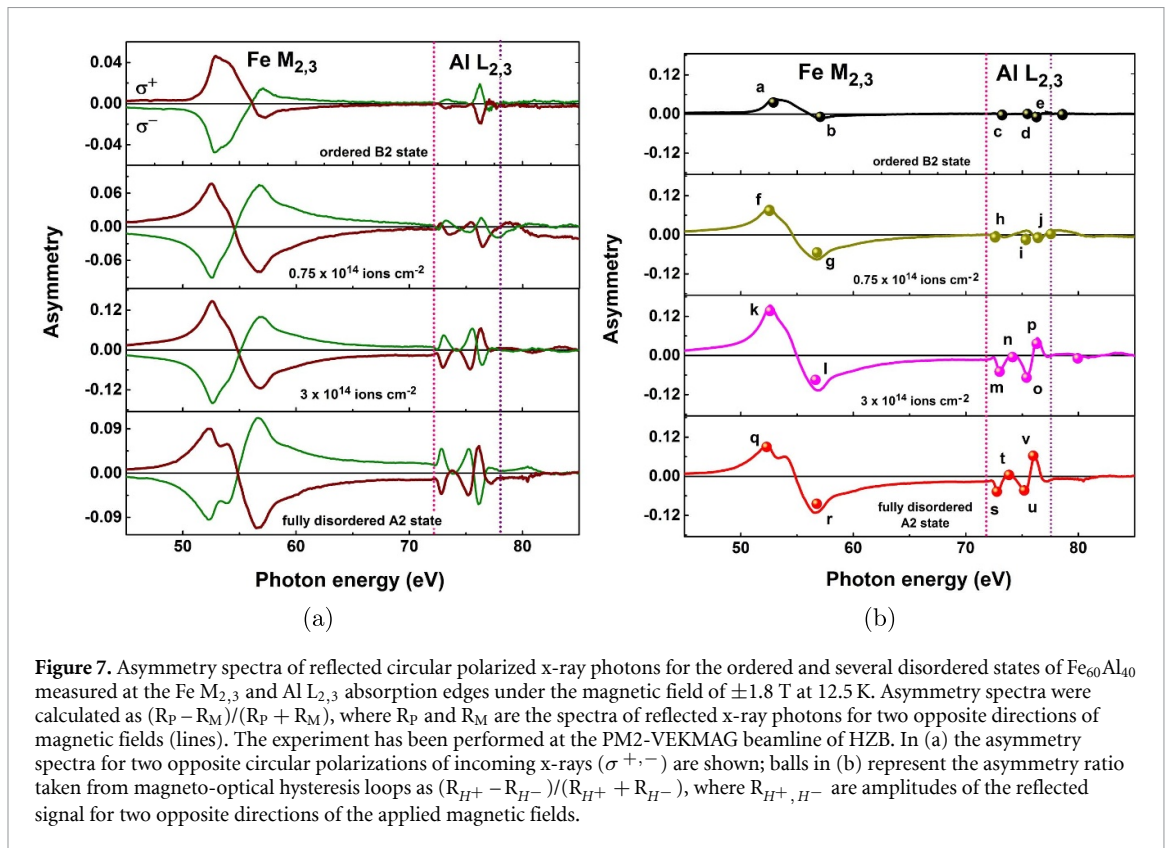
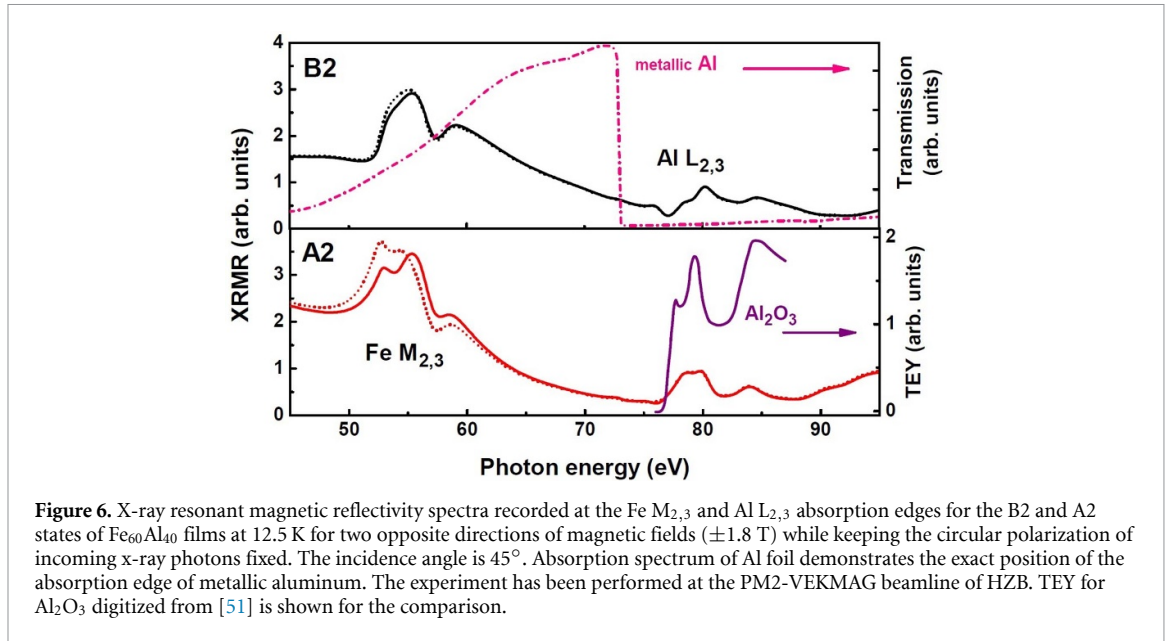
The obvious possibility to prevent FeAl films from the native oxidation by using a capping layer meets at least two types of difficulties. The first one is related to the choice of material for the top layer—it should not contain the elements from the film and should not strongly hybridize with iron; the second one is related to the irradiation process—the presence of the capping layer will form an interface at which an additional mixing of atoms will occur during irradiation by ions. That, in turn, will further affect the magnetic properties of films. A use of light element like Al is not possible due to the first reason, a use of standard capping layer elements like Au or Rh is very questionable due to both of them. In the case of a MgO capping an oxidation of several monolayers of iron is still expected. Thus, a search for a proper material and the thickness of the capping layer is a separate task and will be addressed elsewhere.

3.4. Magnetic polarization of Al

Having one unpaired electron in the valence shell and being placed in the vicinity of the magnetic atoms, aluminum in FeAl alloys and nanoclusters is expected to acquire an induced magnetic polarization owing to Fe–Al hybridization, and up to now there were several theoretical predictions about the existence of a tiny magnetic moment on Al atoms in $\text{Fe}_{1-x}\text{Al}_x$ systems of different stoichiometries [11, 50]. In the present report we demonstrate *experimentally* that Al magnetic polarizations in $\text{Fe}_{60}\text{Al}_{40}$ films are measurable and scales with the degree of the chemical disorder induced by Ne^+ ions.

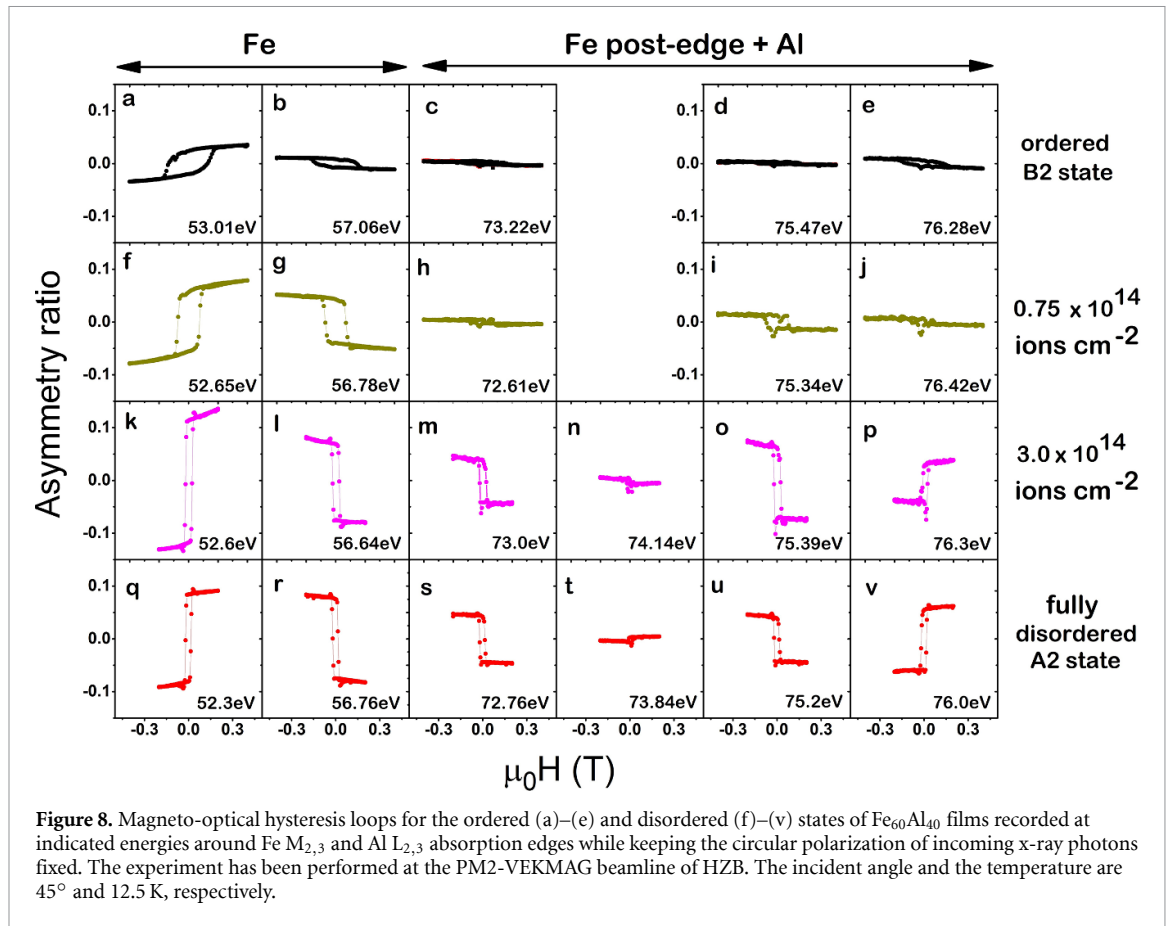
The experimental XRMR spectra of the ordered and the fully disordered $\text{Fe}_{60}\text{Al}_{40}$ phases measured with circularly polarized x-rays for two opposite directions of applied magnetic field at Fe $M_{2,3}$ and Al $L_{2,3}$ edges are presented in figure 6. A rather complex shape of the spectra was found in the whole considered energy range as a result of an interference mixing of structural and magnetic contributions to the reflected signal. The absorption spectrum of Al foil and TEY from $\gamma\text{-Al}_2\text{O}_3$ oxide indicate the positions of metallic and oxidized Al absorption edges, respectively. In spite in the XUV regime the wavelength of the incoming photons is of the order of several *tens* of nm, which is comparable with the total thickness of studied $\text{Fe}_{60}\text{Al}_{40}$ films, the strong contribution from the top oxide layer could not be avoided since the penetration depth of x-ray photons in this range is extremely low and highly dependent on the geometry of the experiment. In the considered cases the probing depth is expected to be up to 5–8 nm which is very similar to the depths probed by XMCD at the Fe $L_{2,3}$ edges. Nevertheless, the magnetic dichroic signal is expected to be visible only from the magnetic atoms in the film (both Fe and Al) and not from the oxide layer as discussed above.

A clear difference in XRMR spectra at the Fe $M_{2,3}$ edges confirms our aforementioned findings at the Fe $L_{2,3}$ ones showing the presence of Fe magnetic moments in the films while only a vanishing difference was found at the Al $L_{2,3}$ edges. To check carefully the magnetic nature of the observed signal, XRMR spectra were measured also for the opposite helicity of incoming x-rays. XRMR asymmetry spectra calculated as



$(R_P - R_M)/(R_P + R_M)$, where R_P and R_M are XRM spectra for two opposite directions of magnetic fields, are introduced to eliminate the non-magnetic contributions and are presented in figure 7(a) for both helicities, σ^+ and σ^- , respectively.

The magnetic asymmetry spectra exhibit a very good reversibility with changing of incoming x-rays polarization validating the presence of magnetic contributions into the reflectivity spectra at all considered edges. Moreover, these asymmetry spectra clearly show magnetic peculiarities for energies associated with metallic Al atoms in the films (the energy range marked by two vertical dashed lines) and not with Al ions in the top oxide layer. This separation is possible due to a significant chemical shift of the absorption edge of Al oxidized states as compared with the metallic Al. Besides, the amplitude of these magnetic peculiarities visibly enlarges for the disordered states created by irradiation of higher fluences.



In figure 7(b) the averaged over both helicities asymmetry spectra are shown along with the asymmetry ratio taken from MO hysteresis loops recorded as reflected intensity changes as a function of external magnetic field at several energies around Fe $M_{2,3}$ and Al $L_{2,3}$ absorption edges to check similarities and distinctions in field dependences of the observed magnetic signals. As seen from the figure, the amplitudes of the asymmetry spectra local extrema are in good agreement with the asymmetry ratio taken from MO hysteresis loops indicating a good reproducibility of the results. Some discrepancies in magnetic asymmetry values found by these two different routes are due to smaller magnetic fields used for the recording of MO hysteresis loops (clearly seen for the Fe $M_{2,3}$ edges) and a competition between a very small magnetic signal arising from Al atoms and a possible post-edge Fe resonance background (for the Al $L_{2,3}$ edges). A slight shift in energy positions of local extrema is due to interference effects and is a common feature of the reflectivity spectra.

A series of the MO hysteresis loops in asymmetry ratio units is presented in figure 8 for the ordered and several disordered states. The shape of the loops follows the same tendency as was previously found in the element-specific hysteresis measured by XMCD at the Fe L_3 edge: a larger coercivity and a more pronounced slope were found for the ordered B2 state (figures 8(a) and (b)) while the coercive field becomes smaller and the magnetic saturation tends to be achieved at smaller fields for the fully disordered A2 one (figures 8(q) and (r)). Intermediate A2 states created by $(0.75 - 3) \times 10^{14}$ ions cm^{-2} fluences reveal in-between quantities (see figures 8(f), (g) and (k), (l)).

At energies associated with metallic Al, which are more than 10 eV above the absorption edge of Fe, in addition to a tiny magnetic signal from Al atoms the contribution from Fe $3p$ resonance is expected. But this contribution to the asymmetry spectra is represented only by a smooth background function and could not be a reason for the observed magnetic fine structure. The resulting signal measured by MO hysteresis loops could either follow the field dependence measured just above the Fe $M_{2,3}$ edges (see figures 8(b), (g), (l) and (r)) or change the sign if the magnetic contribution from Al atoms is large enough as compared to the contribution from Fe moments. As seen from figure 8, for the ordered B2 state (c)–(e) and the disordered state created by irradiation of 0.75×10^{14} ions cm^{-2} fluence ((h)–(j)) no any switching of the asymmetry ratio sign has been found while for the more disordered states created by fluences of $(3-6) \times 10^{14}$ ions cm^{-2} , there is a clear switching (panels p, t and v). Interestingly, the direction of this switching is opposite in comparison with what has been observed at the Fe $M_{2,3}$ edges. Moreover, the coercive fields observed for a

particular ordered or disordered states are found to be very similar for energies associated with Fe and Al atoms indicating a strong coupling between Fe and Al magnetic moments.

The most intriguing question addressed to the MO hysteresis loops is related to the sign of the asymmetry ratio recorded at the Al $L_{2,3}$ edges and its comparison with the sign observed at the Fe $M_{2,3}$ absorption edges. It is well known, that XMCD spectra are especially sensitive to variations in the optical constants (energy-dependent complex index of refraction), dispersive and absorptive parts of which vary significantly at the absorption edges due to the resonant additives. The absorptive part of additives is proportional to the XMCD signal, while the dispersive part could be calculated from the absorptive one via Kramers–Kronig transforms and, thus, shows a derivative-like shape. An example of energy dependences for both parts of resonant additives calculated by Kramers–Kronig transforms could be found e.g. in [25, 52].

If the sign of the XMCD signal changes, the direction of the derivative will change accordingly. As it is seen from figure 7(b) the derivative-like shape of the asymmetry spectra associated with the Fe $M_{2,3}$ absorption edges is opposite to the Al $L_{2,3}$ one. This fact might be an indication of the opposite directions of XMCD signals at these edges. However, due to a very complex formation mechanism of the observed magnetic fine structure in the asymmetry spectra which involves non-resonant (non-magnetic) and resonant (magnetic and non-magnetic) contributions from Fe and Al atoms together with an additional influence of the top oxide layer—no strong conclusions about ferromagnetic or antiferromagnetic coupling of Fe and Al magnetic moments in Fe aluminide films could be done at the moment.

4. Summary and outlooks

The phenomenon of disorder-induced long-range ferromagnetic order created by ion irradiation in $Fe_{60}Al_{40}$ thin films under a control way is very attractive for applications. In combination with patterning, a wide range of spintronic devices that would employ lateral and/or depth-distributed magnetic and structural properties can be created. As a step towards this direction an interrelation between atomic local surrounding and a continuous rise of Fe spin polarization through B2 \rightarrow A2 order-disorder phase transition induced by 20 keV Ne^+ ion irradiation with low fluences ($\sim 10^{14}$ ions cm^{-2}) has been studied by element-specific EXAFS, XANES and XMCD techniques in the soft x-ray energy range.

The structural properties of studied films probed by GIXRD at RT reveal an expanded unit cell together with a disappearance of the ordered fraction already at the intermediate stage of the phase transition. The results point out that the disordered A2 states created by fluences of $(0.75-6) \times 10^{14}$ ions cm^{-2} exhibit strongly different local configurations compared with the ordered B2 state. EXAFS and XANES spectra recorded at the Al K edge at 5 K have confirmed that under the irradiation Al local environment changes, and significant variations in the electronic structure of Al atoms have been found.

XMCD spectra recorded at the Fe $L_{2,3}$ edges at RT show that only non-oxidized Fe atoms in the films bear a visible net magnetic moment. The sum rules analysis has allowed to establish a clear trend of increased spin polarization of Fe $3d$ states. Qualitatively, the same tendency was previously found by macroscopic MOKE. Due to the characteristic depth-profile of disordering created by 20 keV Ne^+ ions and only a surface sensitivity of the soft x-rays the inflection point of magnetic moment fluence-dependence measured by soft x-ray XMCD is shifted to higher fluences in comparison with those measured by MOKE. The main raise of Fe $3d$ magnetic moments takes place in the fluence range below 0.75×10^{14} ions cm^{-2} , where the strongest transformations of Al electronic structure are assumed. A drastic difference in coercive fields revealed by element-specific hysteresis loops at low temperature points on different effective anisotropy fields in films before and after irradiation.

The XRMR experiment performed at the Al $L_{2,3}$ edges discloses the presence of Al atoms magnetic polarization which scales with the degree of the chemical disorder in the studied films. MO hysteresis loops recorded at the Fe $M_{2,3}$ and Al $L_{2,3}$ edges at low temperature confirm the changes of iron coercive fields after the irradiation and show evidence of a strong coupling of Fe and Al magnetic moments.

The attempt to reduce the top oxide layer by an inductively coupled hydrogen plasma has illustrated one more possibility to turn back the order-disorder phase transition in addition to previously reported thermal and laser heating. Such a treatment could be applied for the recovering of the B2-like phase in the surface region of the initially irradiated films. More generally, reduction of surface oxides by hydrogen treatment can be used as an optional cleaning step prior to deposition of subsequent layers in heterostructures relevant to applications. However, a question about the influence of additional layers on the disorder creation, magnetic and dynamic properties of thin films and different types of multilayer devices in the presence of irradiation-induced effects requires further detailed consideration.

Data availability statement

The data that support the findings of this study are available upon reasonable request from the authors.

Acknowledgments

The authors thank the Helmholtz-Zentrum Berlin for provision of access to synchrotron radiation facilities and allocation of synchrotron radiation beamtimes for the experiments at the high field diffractometer end-station at UE46_PGM-1 beamline (Projects 15102122-ST and 15202624-ST/R) and the XRMR experiment in the XUV range at the VEKMAG end-station installed at the PM2-VEKMAG beamline of BESSY II, Helmholtz-Zentrum Berlin (HZB) (Project 182-07609-ST). GIXRD measurements at KMC-2 beamline of HZB are acknowledged in addition. A Smekhova and C Schmitz-Antoniak acknowledge the funding from Helmholtz Association (Young Investigator's Group 'Borderline Magnetism', VH-NG-1031). Besides, A Smekhova is grateful for personal funding from CALIPSOplus project (the Grant Agreement no. 730872 from the EU Framework Programme for Research and Innovation HORIZON 2020). R Bali and H Wende acknowledge funding by the Deutsche Forschungsgemeinschaft (DFG) – 322462997 (BA 5656/1 | WE 2623/14). The authors acknowledge the financial support for the VEKMAG project and for the PM2-VEKMAG beamline by the German Federal Ministry for Education and Research (BMBF 05K10PC2, 05K10WR1, 05K10KE1) and by HZB. A Smekhova, Th Szyjka and B Eggert thankfully acknowledge the financial support from HZB for the travel costs. Steffen Rudorff is acknowledged for technical support.

Appendix. Application of the hydrogen plasma treatment

A.1. Details of the experiment

A low-pressure (10^{-2} mbar) hydrogen plasma treatment has been performed *in situ* with the help of a portable glass plasma chamber attached to the UHV system of UE46_PGM-1 beamline. The generated plasma interacted in normal geometry with samples mounted on the sample holder that was used for x-ray absorption measurements in the high-field end-station of the beamline. The only cycle of 25 min plasma treatment (at pressure of $(2.0 - 2.2) \times 10^{-2}$ mbar) was performed on the unirradiated sample (the initial B2 ordered phase) whereas two sequential cycles of treatment (at pressures of $(2.0 - 3.0) \times 10^{-2}$ mbar and 4.5×10^{-2} mbar, respectively) with a total duration of 50 min were done on the sample irradiated with the highest fluence (the initial fully disordered A2 phase). More details about the construction, advantages, and operation of inductively coupled radio-frequency soft plasma in the aforementioned plasma chamber can be found in [53].

A.2. Results of the soft plasma treatment

Due to its small size hydrogen can penetrate the metallic films deeper than the probing depth of TEY used in XMCD measurements along with initiation of at least two different processes: the reduction of the oxidized Fe ions in the top oxide layer [53, 54] and the dilation of the unit cell. Moreover, our results show that depending on the initial state of the sample that undergo the treatment, a significant drop or a small rise of iron magnetic moment could be achieved in a newly created B2-like ordered phase.

The resulting XANES and XMCD spectra recorded at the Fe $L_{2,3}$ edges at 5 K for the initially ordered and the fully disordered states are presented in figure A1. In both cases the treatment has allowed to significantly clean the surface from natively grown iron oxides till the oxidation peak completely disappeared and the specific shoulders at the high energy side of both absorption edges have been uncovered. This shoulder refers to hybridization effects between Fe and Al, which is analogous to that previously was found in Fe_3Si [55] and Ni_3Al [56]. The small shoulder seen in the XMCD spectra (see inset in figure A1, bottom panel) associated with oxidized Fe ions disappeared after processing of both samples. The amplitude of the XMCD signal for the initially irradiated sample (A2 state) was drastically decreased while the XMCD signal for the initially unirradiated sample (B2 state) was enlarged. The values of iron $3d$ magnetic moments in the films before and after the treatment estimated by the sum rules analysis in the same way as it was done in the main manuscript are presented in table A1.

The element-specific hysteresis loops measured at the Fe L_3 edge at LT after the treatment of the initially unirradiated and the fully irradiated films are presented in figure A2. The obtained shapes of ESHC, coercive fields, the electronic structure of Al absorbers (see e.g. inset in figure A1) as well as the absolute values of the XMCD asymmetry are very similar to those found for the ordered B2 state before the treatment, showing that the processed states are mostly B2-like for both studied films. Nevertheless, different mechanisms of

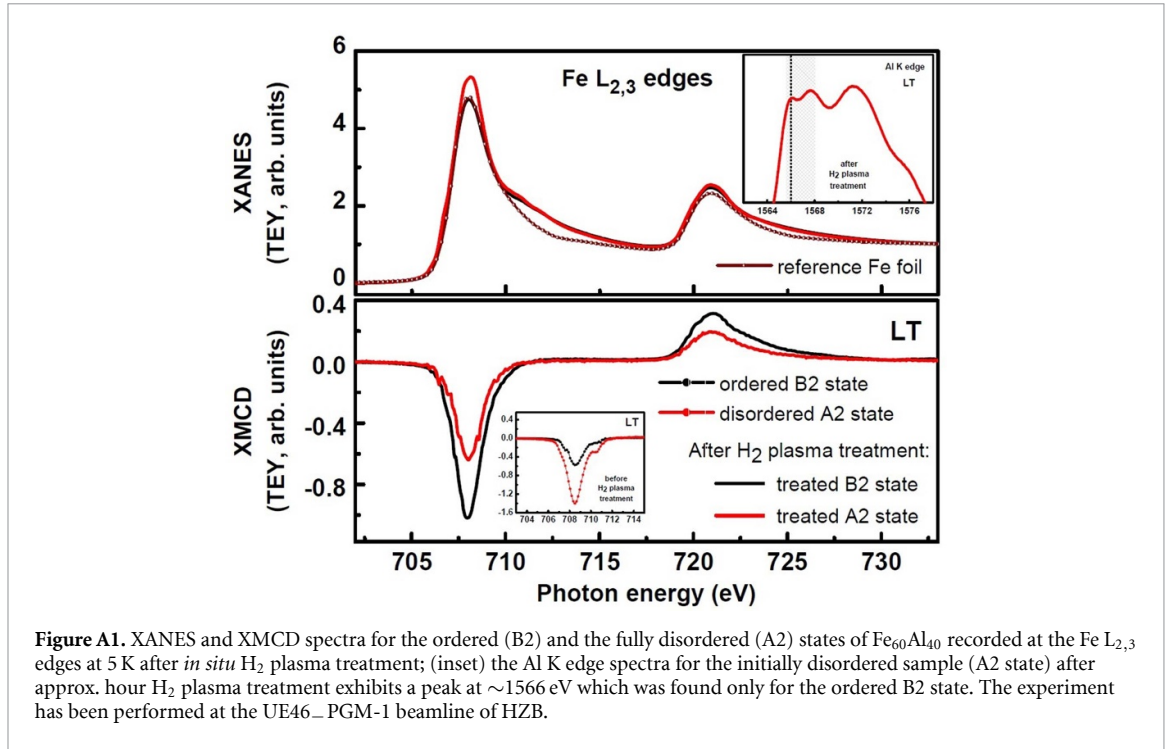
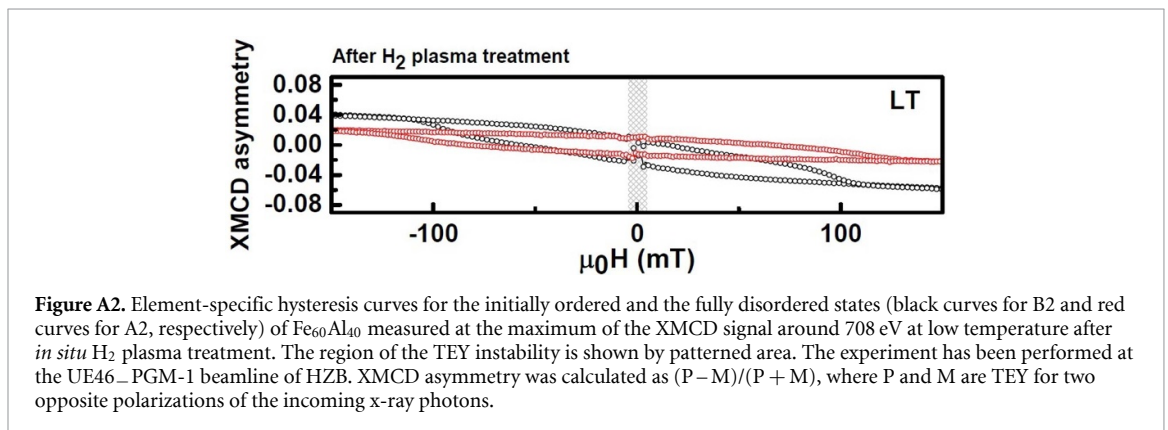


Table A1. The values of Fe $3d$ total magnetic moment (M_{tot}) per $3d$ hole, the number of $3d$ holes, M_{tot} , the effective spin (M_{spin}^*) and orbital (M_{orb}) magnetic moments estimated by the sum rules analysis applied to the XMCD spectra recorded at LT from the unirradiated sample and the sample irradiated by 6×10^{14} ions cm^{-2} fluence before and after hydrogen plasma treatment.

Fluence [ions cm^{-2}]	Ordered B2 state		Fully disordered A2 state	
	LT			
	before treatment	after treatment	before treatment	after treatment
M_{tot} [μ_{Bohr} / $3d$ hole]	0.16(3)	0.23(4)	0.47(9)	0.14(3)
Number of $3d$ holes	3.3(1)	4.0(1)	3.1(1)	4.1(1)
M_{tot} [μ_{Bohr}]	0.53(11)	0.93(19)	1.45(29)	0.57(11)
M_{spin}^* [μ_{Bohr}]	0.50(10)	0.88(18)	1.36(27)	0.54(11)
M_{orb} [μ_{Bohr}]	0.03(1)	0.06(1)	0.09(2)	0.04(1)



formation the resulting magnetic moments are assumed depending on the initial state of the sample. Also, the time of treatment and the plasma base pressure could play a role.

In the initially irradiated sample, the net magnetic moment is determined by the depth profile of the disorder under the top oxide layer. When the treatment is applied, the expansion of the unit cell alters distributions of thermal vacancies which are always present in FeAl systems (in analog of the thermal annealing process) leading to turning back the order-disorder phase transition and a creation of the ordered

phase with a visibly smaller net magnetic moment of Fe atoms contrary to the initially disordered one. The drop of the magnetic moment due to this process is much larger as compared to a small rise of net magnetization determined by iron spins that initially aligned antiferromagnetically in the oxide layer that prior the treatment do not significantly contribute into the XMCD signal due to their preferential antiferromagnetic or ferrimagnetic ordering.

However, for both samples treated by hydrogen plasma, the process of Fe oxides removal from the top is assumed to go in the same manner because the films are chemically identical and have a very similar native oxide layer with only slightly different thicknesses. Upon a creation of the new B2-like phase instead of the Fe oxide, oxygen ions are taken out by hydrogen while Fe atoms stay. Thus, a contribution into the iron net magnetization from the top region appears when the whole film is magnetically saturated. Since the initially unirradiated sample is dominantly in the ordered B2 state, this additional contribution will increase the value of Fe magnetic moment per atom.

As follows from above, the important peculiarities of the initially ordered state found by soft x-ray absorption spectroscopy at low temperature—the characteristic peak in the Al K edge XANES region, low net magnetic moment of iron and enhanced coercivity of ESHC—are related to the ordered B2 state of Fe₆₀Al₄₀ film itself and not to the presence of the top oxide layer. The results suggest that the soft plasma treatment can be effectively used for turning back the irradiated films into the ordered state, but the current data do not allow to make quantitative conclusions about systematic changes of iron magnetic moments. Therefore, the question about influence of oxides removal on electronic and magnetic properties of constituent atoms in Fe₆₀Al₄₀ thin films depending on hydrogen treatment conditions needs to be additionally studied in details.

ORCID iDs

B Eggert  <https://orcid.org/0000-0001-7739-3541>

F Wilhelm  <https://orcid.org/0000-0002-4425-3662>

References

- [1] Huffman G P and Fisher R M 1967 *J. Appl. Phys.* **38** 735–42
- [2] Nevitt M and Aldred A 1963 *J. Appl. Phys.* **34** 463–8
- [3] Aldred A, Rainford B, Kouvel J and Hicks T 1976 *Phys. Rev. B* **14** 228–34
- [4] Shirane G, Chen C, Flinn P and Nathans R 1963 *Phys. Rev.* **131** 183–90
- [5] Fassbender J, Liedke M O, Strache T, Möller W, Menéndez E, Sort J, Rao K V, Deevi S C and Nogués J 2008 *Phys. Rev. B* **77** 174430
- [6] Kelly D, Schuller I, Korenivski V, Rao K, Larsen K, Bottiger J, Gyorgy E and van Dover R 1994 *Phys. Rev. B* **50** 3481(R)–84(R)
- [7] Tohki A, Aikoh K, Iwase A, Yoneda K, Kosugi S, Kume K, Batchuluun T, Ishigami R and Matsui T 2012 *J. Appl. Phys.* **111** 07A742
- [8] Sato H and Arrott A 1959 *Phys. Rev.* **114** 1427–40
- [9] Yelsukov E, Voronina E and Barinov V 1992 *J. Magn. Magn. Mater.* **115** 271–80
- [10] Bogner J, Steiner W, Reissner M, Mohn P, Blaha P, Schwarz K, Krachler R, Ipser H and Sepiol B 1998 *Phys. Rev. B* **58** 14922–33
- [11] Kulikov N I, Postnikov A V, Borstel G and Braun J 1999 *Phys. Rev. B* **59** 6824–33
- [12] Nogués J et al 2006 *Phys. Rev. B* **74** 024407
- [13] Bali R et al 2014 *Nano Lett.* **14** 435–41
- [14] Tahir N et al 2014 *IEEE Trans. Magn.* **50** 1–4
- [15] Röder F, Hlawacek G, Wintz S, Hübner R, Bischoff L, Lichte H, Potzger K, Lindner J, Fassbender J and Bali R 2015 *Sci. Rep.* **5** 16786
- [16] Liedke M O et al 2015 *J. Appl. Phys.* **117** 163908
- [17] Yoshida Y, Oosawa K, Watanabe S, Kaiju H, Kondo K, Ishibashi A and Yoshimi K 2013 *Appl. Phys. Lett.* **102** 183109
- [18] Ehrler J et al 2018 *ACS Appl. Mater. Interfaces* **10** 15232–9
- [19] La Torre E et al 2018 *Phys. Rev. B* **98** 024101
- [20] Thole B T, Carra P, Sette F and van der Laan G 1992 *Phys. Rev. Lett.* **68** 1943–6
- [21] Carra P, Thole B T, Altarelli M and Wang X 1993 *Phys. Rev. Lett.* **70** 694–7
- [22] Tonnerre J M, Séve L, Raoux D, Soullié G, Rodmacq B and Wolfers P 1995 *Phys. Rev. Lett.* **75** 740–3
- [23] Mertins H C, Abramsohn D, Gaupp A, Schäfers F, Gudat W, Zaharko O, Grimmer H and Oppeneer P M 2002 *Phys. Rev. B* **66** 184404
- [24] Stöhr J and Siegmann H C 2006 *Magnetism (Springer Series in Solid-State Sciences vol 152)* (Springer)
- [25] Macke S and Goering E 2014 *J. Phys.: Condens. Matter.* **26** 363201
- [26] Valencia S, Gaupp A, Gudat W, Mertins H-C, Oppeneer P M, Abramsohn D and Schneider C M 2006 *New J. Phys.* **8** 254–254
- [27] Grychtol P, Adam R, Valencia S, Cramm S, Bürgler D E and Schneider C M 2010 *Phys. Rev. B* **82** 054433
- [28] Többens D and Zander S 2016 *J. Large-Scale Res. Facil.* **2** A49
- [29] Englisch U, Rossner H, Maletta H, Bahrdr J, Sasaki S, Senf F, Sawhney K and Gudat W 2001 *Nucl. Instrum. Methods Phys. Res. A* **467–468** 541–4
- [30] Schmitz D et al 2002 *BESSY Annu. Rep.* **10** 358–61
- [31] Noll T and Radu F 2017 The mechanics of the VEKMAG experiment *Proc. Mechanical Engineering Design of Synchrotron Radiation Equipment and Instrumentation Conf. (MEDSI'16) (Barcelona, Spain, 11–16 September 2016) Mechanical Engineering Design of Synchrotron Radiation Equipment and Instrumentation Conf.* pp 370–3
- [32] Mogi M, Yamamoto T, Mizoguchi T, Tatsumi K, Yoshioka S, Kameyama S, Tanaka I and Adachi H 2004 *Mater. Trans.* **45** 2031–4
- [33] Altman A B et al 2017 *Inorg. Chem.* **56** 5710–9
- [34] Botton G A, Guo G Y, Temmerman W M and Humphreys C J 1996 *Phys. Rev. B* **54** 1682–91
- [35] Shimizu K, Kato Y, Yoshida T, Yoshida H, Satsuma A and Hattori T 1999 *Chem. Commun.* 1681–2

- [36] Richard N, Lequeux N, Cortes R and Florian P 1997 *J. Phys. IV* **7** C2–1069–C2–1071
- [37] Leon A, Balerna A, Cinque G, Frommen C and Fichtner M 2007 *J. Phys. Chem.* **111** 3795–8
- [38] Fauth K, Goering E, Schütz G and Kuhn L 2004 *J. Appl. Phys.* **96** 399
- [39] Signorini L, Pasquini L, Boscherini F, Bonetti E, Letard I, Brice-Profeta S and Sainctavit P 2006 *Phys. Rev. B* **74** 014426
- [40] Boyen H G et al 2005 *Adv. Mater.* **17** 574–8
- [41] Antoniak C et al 2006 *Phys. Rev. Lett.* **97** 117201
- [42] Powell C J 1974 *Surf. Sci.* **44** 29–46
- [43] Nakajima R, Stöhr J and Idzerda Y 1999 *Phys. Rev. B* **59** 6421–9
- [44] Stöhr J and Siegmann H C 2006 *Magnetism: From Fundamentals to Nanoscale Dynamics* (Springer)
- [45] Frazer B H, Gilbert B, Sonderegger B R and Stasio G D 2003 *Surf. Sci.* **537** 161–7
- [46] Ziegler J F, Ziegler M and Biersack J 2010 *Nucl. Instrum. Methods Phys. Res. B* **268** 1818–23
- [47] Aikoh K, Tohki A, Okuda S, Saitoh Y, Kamiya T, Nakamura T, Kinoshita T, Iwase A and Matsui T 2013 *Nucl. Instrum. Methods Phys. Res. B* **314** 99–102
- [48] Pizzini S, Fontaine A, Dartyge E, Giorgetti C, Baudelet F, Kappler J P, Boher P and Giron F 1994 *Phys. Rev. B* **50** 3779–88
- [49] Mathon O, Baudelet F, Itié J P, Pasternak S, Polian A and Pascarelli S 2004 *J. Synchrotron Radiat.* **11** 423–7
- [50] Das G P, Rao B K, Jena P and Deevi S C 2002 *Phys. Rev. B* **66** 184203
- [51] Filatova E O, Konashuk A S, Sakhonenkov S S, Sokolov A A and Afanašev V V 2017 *Sci. Rep.* **7** 4541
- [52] Kortright J B and Kim S K 2000 *Phys. Rev. B* **62** 12216–28
- [53] Schmitz-Antoniak C, Schmitz D, Warland A, Svechkina N, Salamon S, Piamonteze C and Wende H 2016 *Sci. Rep.* **6** 20897
- [54] Schmitz-Antoniak C, Izarova N, Svechkina N, Smekhova A, Stuckart M, Schmitz D and Kögerler P 2019 *Eur. J. Inorg. Chem.* **2019** 448–55
- [55] Krumme B et al 2009 *Phys. Rev. B* **80** 144403
- [56] Chang Y K, Lin K P, Pong W F, Tsai M H, Hseih H H, Pieh J Y, Tseng P K, Lee J F and Hsu L S 2000 *J. Appl. Phys.* **87** 1312–7
- [57] Rogalev A, Wilhelm F, Goulon J and Goujon G 2013 *Advanced instrumentation for x-ray magnetic circular dichroism Magnetism and Synchrotron Radiation: Towards the Fourth Generation Light Sources* ed E Beaurepaire, H Bulou, L Joly and F Scheurer (Springer) pp 289–314